

# Extended-Depth-of-Field Iris Recognition Using Unrestored Wavefront-Coded Imagery

Vishnu Naresh Boddeti, *Student Member, IEEE*, and B. V. K. Vijaya Kumar, *Fellow, IEEE*

**Abstract**—Iris recognition can offer high-accuracy person recognition, particularly when the acquired iris image is well focused. However, in some practical scenarios, user cooperation may not be sufficient to acquire iris images in focus; therefore, iris recognition using camera systems with a large depth of field is very desirable. One approach to achieve extended depth of field is to use a wavefront-coding system as proposed by Dowski and Cathey, which uses a phase modulation mask. The conventional approach when using a camera system with such a phase mask is to restore the raw images acquired from the camera before feeding them into the iris recognition module. In this paper, we investigate the feasibility of skipping the image restoration step with minimal degradation in recognition performance while still increasing the depth of field of the whole system compared to an imaging system without a phase mask. By using a simulated wavefront-coded imagery, we present the results of two different iris recognition algorithms, namely, Daugman's iricode and correlation-filter-based iris recognition, using more than 1000 iris images taken from the Iris Challenge Evaluation database. We carefully study the effect of an off-the-shelf phase mask on iris segmentation and iris matching, and finally, to better enable the use of unrestored wavefront-coded images, we design a custom phase mask by formulating an optimization problem. Our results suggest that, in exchange for some degradation in recognition performance at the best focus, we can increase the depth of field by a factor of about four (over a conventional camera system without a phase mask) by carefully designing the phase masks.

**Index Terms**—Challenging iris recognition, correlation filters, extended depth of field, wavefront coding.

## I. INTRODUCTION

THE performance of an iris recognition system depends greatly on how well the iris acquisition system captures the texture detail which generally requires the iris to be within the focus volume of the acquisition system. Hence, conventional iris image acquisition systems require user cooperation to a large extent in positioning the head so that the eyes are located within the focus volume of the imaging system. Therefore, an iris acquisition system with a greater depth of field provides us greater flexibility and robustness. Furthermore, camera systems estimate the position of the user by adjusting the pan, tilt, and focus, which is usually not perfect. Having a greater depth of

field (defined as the distance range from the camera over which the subject is acceptably sharp in the image) makes this task easier for the camera system.

The traditional solution to increased depth of field is to increase the  $f$  number of the lens. This translates to using a smaller aperture which, in turn, may decrease—depending on the sensor pixel size—the effective resolution of the camera system due to diffraction and also reduce the amount of light captured by the sensor, thereby hurting the signal-to-noise ratio. The light level can be increased by increasing the exposure time. Increased exposure time, however, introduces motion blur since it would be unrealistic to expect the eyes to be perfectly still for the increased duration of the exposure.

One way to achieve extended depth of field without sacrificing aperture size is to take advantage of computational imaging which combines optics with digital signal processing. To extend the depth of focus of an imaging system, Dowski and Cathey [1], [2] proposed the use of a phase mask. The idea is to use phase modulation to increase focus tolerance along the axis of the lens. Under misfocus, the modulation transfer function (MTF) of a conventional optical system goes to zero at some frequencies. In addition, the shape of the MTF under misfocus is significantly different from the shape of the MTF in focus (see Fig. 1). On the other hand, the MTF of a wavefront-coding system does not have any nulls over a broad range of misfocus, and the shape of the MTF under misfocus does not change appreciably compared to that under the best focus (see Fig. 2). Both these properties can be exploited to increase the depth of field of an iris recognition system.

Avoiding MTF nulls is attractive since, in this case, there are no frequencies which are irretrievably lost, thereby preserving all the information in the signal. Therefore, at least in theory, we can recover the original information and achieve greater depth of field at the same time. The effect of wavefront coding can be modeled as a linear operation on an image obtained from a conventional camera; therefore, any iris recognition algorithm, which is tolerant to such linear operations, is an attractive candidate when using wavefront-coded imagery. Many correlation filters (such as the minimum average correlation energy (MACE) filter [3]) can compensate for any information-preserving linear operation [4] as long as the same linear operation is applied on both the gallery and the probe images, making correlation filters very attractive for this task. At the same time, the popular iricode algorithm [5]–[7] also has some tolerance to the phase modulation caused by wavefront coding since the algorithm depends only on quantized phase values (four quantization levels) of local Gabor wavelet responses.

Manuscript received December 5, 2008; revised May 27, 2009. First published March 22, 2010; current version published April 14, 2010. This paper was recommended by Guest Editor K. W. Bowyer.

The authors are with the Department of Electrical and Computer Engineering, Carnegie Mellon University, Pittsburgh, PA 15213 USA (e-mail: naresh@cmu.edu).

Color versions of one or more of the figures in this paper are available online at <http://ieeexplore.ieee.org>.

Digital Object Identifier 10.1109/TSMCA.2010.2041661

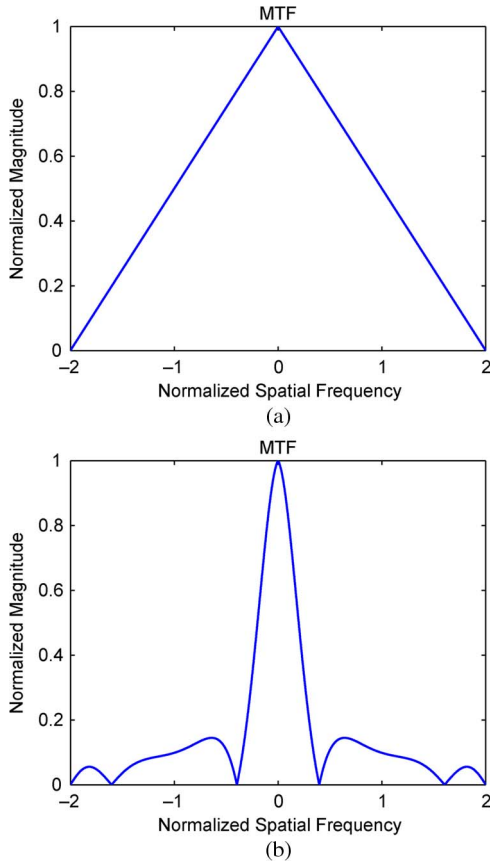


Fig. 1. MTF of conventional camera. (a) MTF of a conventional 1-D aperture in focus. (b) MTF of a conventional 1-D aperture with misfocus parameter  $\psi = \pi^2/2$  [see (9)].

Previous evaluations [8]–[10] on using wavefront coding for iris recognition have demonstrated that using wavefront-coded imagery for iris recognition can increase the depth of field of the whole system without adversely affecting the recognition accuracy. Most of these evaluations were done on a small and carefully selected data set having both real and simulated images. Building upon this, we aim to accomplish the following goals in this paper.

- 1) Evaluate the performance of iris recognition when using wavefront-coded imagery on a large data set.
- 2) Systematically study the effect of wavefront coding on different parts of the iris recognition pipeline.
- 3) Usually, wavefront-coded images are restored before being used for recognition. This image restoration process is computationally expensive, thereby slowing down the iris recognition process. Thus, in this paper, we wish to study the feasibility of using raw (i.e., unrestored) image outputs from the camera directly, relying on the robustness of the recognition algorithms to handle the blurring caused by wavefront coding. Skipping the image restoration step helps in avoiding the computational complexity and hardware required for performing this task.
- 4) Lastly, we would like to compare the performance of two different iris recognition algorithms (iriscode [5] and correlation-filter-based method [11]) when using wavefront-coded imagery.

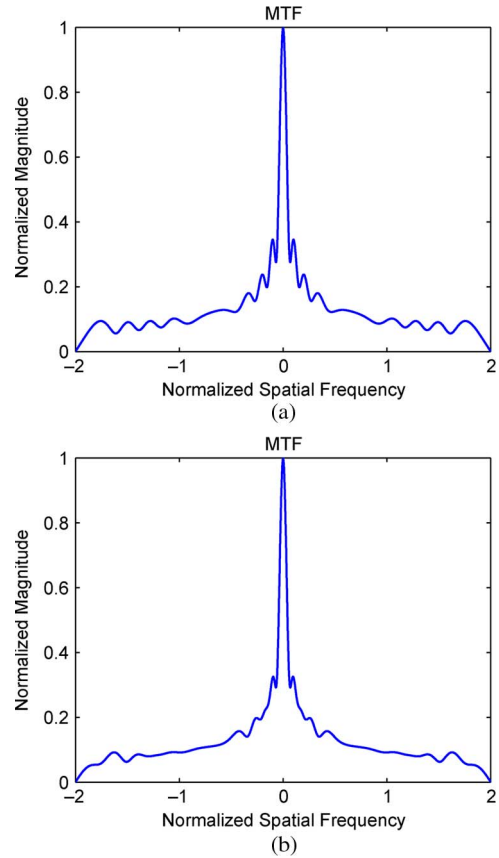


Fig. 2. MTF of wavefront-coded camera. (a) MTF of a 1-D wavefront-coded aperture in focus. (b) MTF of a 1-D wavefront-coded aperture with misfocus parameter  $\psi = \pi^2/2$  [see (9)].

Since there is no publicly available data set of wavefront-coded imagery with a large number of images, we use simulated images in our experiments. For this purpose, we choose our images from the Iris Challenge Evaluation (ICE) [12] database (see Section V for more details on how the images were chosen). It must be noted that, in the images so selected, it is possible that the iris was not in the focal plane of the camera system when capturing the original images. Therefore, the images obtained by simulation would be a convolution of the original image by the simulated point spread function (PSF) and the PSF of the unknown camera system that generated the original image. Similarly, the noise that is added during simulation would be on top of the noise added while capturing the original image. This is the main limitation of our use of simulated iris imagery; therefore, the conclusions we draw from our experiments would be conservative, and the actual performance might be better on real wavefront-coded imagery. Having said that, simulated imagery does provide us with flexibility in how many different types of experiments we can conduct and also in studying the effect of wavefront coding on various aspects of the recognition algorithm. For instance, we can obtain coded images at any desired distance from the camera and with any desired resolution along the optical axis. Furthermore, by using simulated imagery, one can easily evaluate the effect of changing the parameters of the wavefront-coding mask and the type of mask itself.

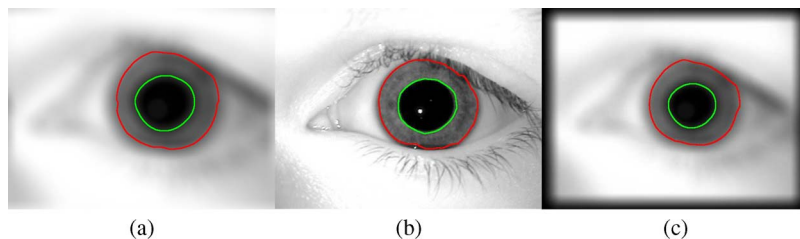


Fig. 3. Examples of iris segmentation on conventional images. (a)  $-4$  cm. (b)  $0$  cm. (c)  $+4$  cm.

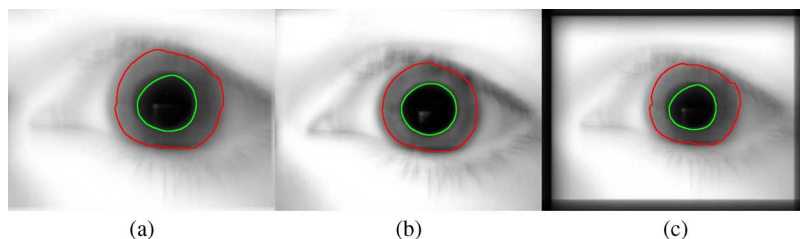


Fig. 4. Examples of iris segmentation on wavefront-coded images. (a)  $-5$  cm. (b)  $0$  cm. (c)  $+5$  cm.

Since the overall performance, both in terms of depth of field and recognition accuracy, is affected by the following two aspects of the iris recognition pipeline, we investigate them separately to fully understand the advantages and challenges of using wavefront coding in iris acquisition systems.

- 1) The blurriness caused by wavefront coding affects iris segmentation, which, in turn, affects the recognition accuracy.
- 2) Due to the phase modulation introduced by wavefront coding, the iris texture undergoes an approximately linear transformation which is reversible via a linear reconstruction. However, noise prevents this reconstruction from being perfect. This linear transformation has an adverse effect on the recognition accuracy unless accounted for by the matching algorithm.

From here onward, we will refer to two types of iris images: Conventional images are those obtained without any wavefront coding, and wavefront-coded images refer to the raw output images (i.e., without restoring the wavefront-coded images) from an imaging system employing wavefront coding.

The rest of this paper is organized as follows. We first describe the preprocessing done to the iris images followed by the feature extraction employed. Next, we describe the two kinds of matching that we compare, namely, iriscodes and correlation filters. Then, we describe how we simulate the iris image data and discuss the recognition results on these simulated data. Finally, we conclude with some observations and analysis of our results.

## II. PREPROCESSING

Before we extract texture features or perform matching, we preprocess the iris images, which involves segmentation and normalization of the iris to be able to compare iris images of different size, and finding and masking of eyelashes and any specularities.

### A. Segmentation

The performance of iris recognition systems is greatly dependent on the ability to isolate the iris from the other parts of the eye such as eyelids and eyelashes. Commonly used iris segmentation techniques use some variant of edge detection methods, and since the blurring introduced by both conventional misfocus and by wavefront coding smudges the edge information to the point of there not being a discernible edge, iris segmentation becomes a challenging task. To alleviate this problem, we use a region-based active contour segmentation [13]. This technique segments the image based on the intensity distribution of a region rather than looking for sharp edges, making it more robust to blurring than an edge-based method. Figs. 3 and 4 show some of our segmentation results on iris images (obtained via the simulations, to be explained in Section V) at various distances from the focal plane of the camera system. Note that, at  $0$  cm (all distances are relative to the focal plane), conventional iris images exhibit more details than wavefront-coded images. However, over the distance ranges shown, conventional iris images exhibit more variability than wavefront-coded iris images.

### B. Normalization

Once the iris boundaries have been found, we map the iris pattern into the polar domain as is popularly done. This has two effects.

- 1) It normalizes different irises to the same size, thus allowing for proper matching.
- 2) Any rotation of the iris manifests as a cyclic shift (along the angular axis) in the polar domain, which can be handled easily by both correlation filters and iriscodes (via circular shifts).

## III. FEATURE EXTRACTION

Gabor filters with carefully selected parameters have been shown to be the most discriminative bandpass filters for iris

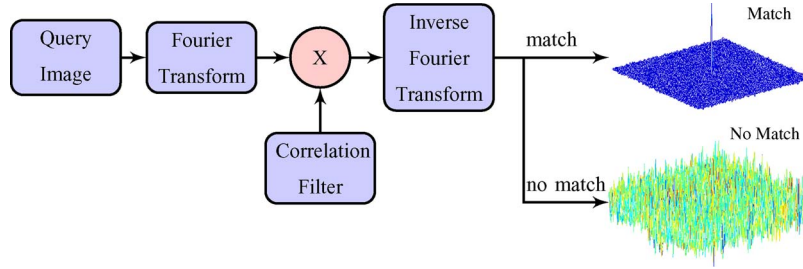


Fig. 5. Application of correlation filter on a query image.

image feature extraction among a variety of wavelet candidates [14]. A Gabor filter is a modulated Gaussian envelope and is given by

$$g(\rho, \phi) = \exp \left[ -\frac{1}{2} \left( \frac{\rho^2}{\sigma_\rho^2} + \frac{\phi^2}{\sigma_\phi^2} \right) - j\rho(\omega \sin \theta) - j\phi(\omega \cos \theta) \right] \quad (1)$$

in the polar domain  $(\rho, \phi)$  where the filter is applied to the iris pattern. Here,  $\theta$  denotes the wavelet orientation,  $\sigma_\rho$  and  $\sigma_\phi$  denote the wavelet extents in the radial and angular directions, respectively, and  $\omega$  denotes the modulation frequency of the wavelet. By varying these parameters, the filters can be tuned to extract features at different scales, rotations, frequencies, and translations. We use a set of these differently localized Gabor filters as our feature extraction filter bank. The filter bank used in our experiments has two scales and four orientations for a total of eight channels, and features are extracted at every point of the unwrapped iris (Daugman's method uses only 1024 Gabor filters). More details on the parameters of the Gabor filters used and how they were chosen can be found in [14]. We also divide the unwrapped iris into multiple (42 in our experiments) patches when using correlation filters for matching, and the projections of these patches onto the Gabor bases yield our features. We finally combine the recognition cues (correlation peak sharpness metrics) of each patch to come up with a final match score. Another point to note is that the bandpass filters we use for feature extraction have been optimized on in-focus conventional iris images, and we use the same Gabor filters throughout our experiments.

#### IV. MATCHING

One of the goals of this paper is to compare the performance of the popular iriscodes method of matching with correlation-filter-based matching in terms of robustness to segmentation errors, robustness to blurring caused in a conventional iris acquisition system, and robustness to blurring caused by wavefront coding.

##### A. Iriscodes

The phase of the complex Gabor wavelet projections obtained, as explained in the previous section, is quantized to 2 b by mapping the phase to one of the four quadrants in the complex plane. All the bits obtained this way constitute an iriscodes. It must be noted that, while it was not the original intent, this phase quantization also provides robustness to the

phase modulation introduced by the wavefront-coding system since there would be errors in the bits only when the phase modulation is large enough to cause the phase to change and fall into another quadrant. Any two irises are compared by matching their respective iriscodes. The matching is done by computing the normalized Hamming distance between the two binary iriscodes. There are also corresponding masks to identify which bits in the iriscodes to use for matching. The mask bits are set to either one or zero, depending on whether the corresponding iriscodes bits are used or not used (e.g., due to eyelid occlusions) for matching. When matching two iriscodes  $A$  and  $B$  with respective masks  $m_A$  and  $m_B$ , the dissimilarity  $d$  is defined as

$$d = \frac{\|(A \oplus B) \cap m_A \cap m_B\|}{\|m_A \cap m_B\|} \quad (2)$$

where  $\oplus$  denotes an XOR operation and  $\| \cdot \|$  denotes the weight (i.e., the number of nonzero elements) of the binary pattern. Rotation of the eye is compensated for by matching the iriscodes at different circular shifts along the angular axis and taking the minimum normalized Hamming distance value.

##### B. Correlation Filters

A correlation filter is a spatial frequency domain array (loosely called a template) that is specifically designed to recognize a particular pattern class represented by a set of reference patterns [15], [16]. A given query pattern is matched against this template by performing a cross-correlation. To make this efficient, the cross-correlation is performed in the frequency domain, taking advantage of the fast Fourier transform

$$C(x, y) = FT^{-1} \{ FT \{ I(x, y) \} \cdot F^*(u, v) \} \quad (3)$$

where  $I(x, y)$  is a query pattern and  $F(u, v)$  is the frequency domain array representing the correlation filter. The resulting cross-correlation output  $C(x, y)$  should contain a sharp peak if the query is authentic and no such peak if it is an impostor as shown in Fig. 5.

The principal advantages of using correlation filters are the following.

- 1) Generation of the whole correlation plane in one shot.
- 2) Graceful performance degradation in the presence of noise or occlusions.
- 3) It can be designed to tolerate a variety of within-class variations.
- 4) Closed-form solutions for the filters.

To quantify the degree of sharpness of the correlation peak, we use the peak-to-correlation energy (PCE) ratio defined as

$$PCE = \frac{\text{peak} - \mu}{\sigma} \quad (4)$$

where  $\mu$  and  $\sigma$  are the mean and standard deviation of the correlation plane, respectively.

There are a variety of advanced correlation filters to choose from [17]. Among these, MACE [3] filter and optimal tradeoff synthetic discriminant function (OTSDF) filter [18] (a more general form of MACE filter) have been found to perform well when applied to the problems of face, fingerprint, and iris recognition [19]–[21]. In this paper, we use the OTSDF filter which provides an optimal tradeoff between the average correlation energy (ACE) and the output noise variance (ONV). The ACE is the energy in the correlation plane averaged over the training images, and minimizing ACE suppresses the side-lobes, resulting in sharp correlation peaks. Minimizing ONV improves the filter's tolerance toward noise. Formulating this in a Lagrangian framework yields a closed-form solution for the optimal tradeoff filter.

The iris patterns are represented as multichannel features, with each channel being the response of one Gabor filter, from our filter bank to the iris image. Thus, we can design one filter for each channel and combine the resulting correlation plane outputs. However, one can do better by jointly optimizing the  $K$  filters [22]; such filters are referred to as “fusion correlation filters.” This leads to

$$H = A^{-1}X(X^+A^{-1}X)^{-1}u \quad (5)$$

where  $H$  is the frequency domain representation of the correlation filter and  $A = \alpha S + (1 - \alpha)\bar{P}$ , with  $S$  being the cross-power spectral density matrix of the noise in the channels and  $\bar{P}$  being the mean cross-power spectral density between the different feature channels. The parameter  $\alpha$  trades off peak sharpness for distortion tolerance. See [11] for more details on fusion OTSDF design and use.

## V. SIMULATIONS

### A. Database

In this paper, we use only a subset of the ICE data set. Sixty one subjects were manually selected such that most of the images of these subjects are either in focus or close to being in focus (i.e., within the depth of field of the actual camera used). We avoided subjects with only one image in the database and subjects with heavy eyelash occlusions. This was done since the main goal of this paper is to evaluate the performance of the iris recognition methods when using extended depth of field methods, and we should avoid other degradation factors such as heavy eyelid/eyelash occlusion affecting the evaluation. In total, our evaluation was done on 1061 images. The chosen images have been used to simulate both the wavefront-coded images and the conventional out-of-focus images. Figs. 6 and 7 show some sample images.

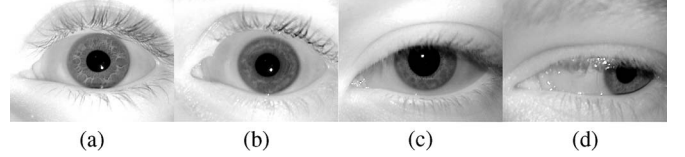


Fig. 6. Examples of ICE images used for evaluation.

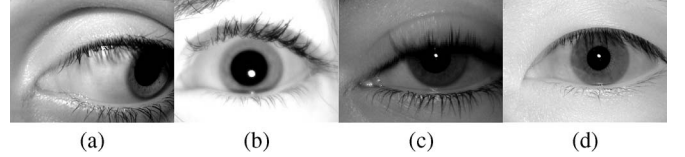


Fig. 7. Examples of ICE images not used for evaluation. (a) Iris too close to the image boundary, which would get cropped out when simulating images closer to the camera due to image magnification. (b) Badly out of focus. (c) Very low contrast between pupil and iris along with eyelid shadow. (d) Eyelashes on the iris.

### B. Simulation Methodology

The simulation of conventional defocus and wavefront-coded imaging was done by convolving the in-focus images with the PSF of both normal and wavefront-coded imaging systems after accounting for the magnification in the image on account of the iris being closer or farther from the camera. This is given by

$$g = h * r + \eta \quad (6)$$

where  $g$  is the blurred and noisy output image,  $h$  is the PSF of the imaging system,  $r$  is the ground truth image, and  $\eta$  is the Poisson noise which, following the common model [23], is given by

$$\eta = \sqrt{h * r} \eta_1 + \sigma \eta_2 \quad (7)$$

where  $\eta_1$  and  $\eta_2$  are zero-mean unit-variance Gaussian random variables and  $\sigma$  is the standard deviation of the image-independent noise.

The PSF model used for the two types of imagery is as given in (8) and (10).

Conventional System:

$$h = \left| FT \left\{ P(x, y) e^{i\psi(x^2+y^2)} \right\} \right|^2 \quad (8)$$

where  $P(x, y)$  is one inside the lens system pupil and zero outside, and the misfocus parameter  $\psi$  is given by

$$\psi = \frac{\pi L^2}{4\lambda} \left( \frac{1}{f} - \frac{1}{d_o} - \frac{1}{d_i} \right) \quad (9)$$

where  $L$  is the lens pupil diameter,  $\lambda$  is the wavelength of light used,  $f$  is the focal length of the lens,  $d_o$  is the object distance from the first principal plane of the lens, and  $d_i$  is the distance between the second principal plane of the lens and the image plane.

Wavefront-Coding System:

$$h = \left| FT \left\{ P(x, y) e^{i(\psi(x^2+y^2)+\phi(x, y))} \right\} \right|^2 \quad (10)$$

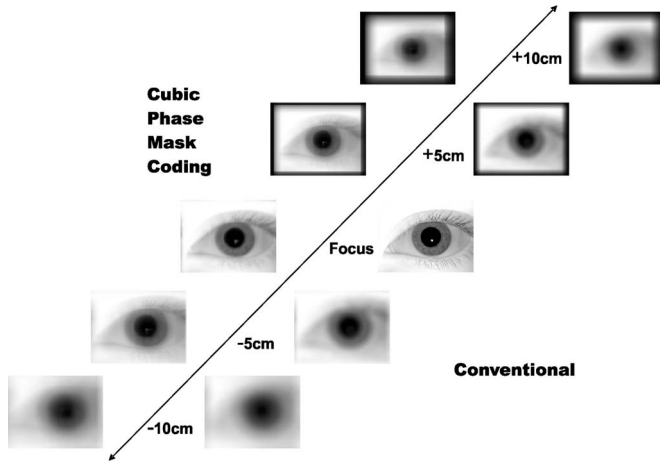


Fig. 8. Sample simulated images of both conventional and wavefront-coded (cubic phase mask with  $\beta = 30$ ) optical systems.

where  $\phi(x, y)$  is the phase function of the mask. We can see that the PSF has two components, namely, the quadratic term which comes from a conventional system and the phase function of the wavefront-coding element. The camera parameters for our database have been chosen based on published literature [8]–[10].

### C. Sample Images

The images were simulated using a cubic phase mask (see Section VI) to cover a distance of 20 cm in either direction from the focal plane with a step size of 1 cm. Fig. 8 shows some sample simulated iris images at various distances.

## VI. EXPERIMENTS AND RESULTS

In this section, we present the results of recognition experiments of iriscodes as well as correlation-filter-based iris pattern matching. These experiments, a total of five, have been designed to answer the following questions.

- 1) Can the depth of field of the iris recognition system be increased using unrestored wavefront-coded imagery?
- 2) What is the impact of wavefront coding on different parts of the iris recognition pipeline, namely, iris segmentation and matching accuracy?
- 3) What are the bottlenecks impacting recognition performance when using unrestored wavefront coding?
- 4) Can a custom phase mask be designed which is optimized for best recognition accuracy when using unrestored wavefront imagery?

For each experiment, we evaluate the impostor and authentic score statistics (mean and standard deviation of match scores plotted as small squares and vertical bars, respectively) to determine the improvement in the imaging distance obtained compared to the conventional iris imaging system.

To answer the first three questions, we use a cubic phase mask  $\phi(x, y) = \beta(x^3 + y^3)$ , for consistency with earlier work. Fig. 9 shows the PSF over a range of distances from the focal plane.

### A. Experiment I(a)

In this experiment, we use in-focus images, both conventional and wavefront-coded (cubic phase mask with  $\beta = 30$ ), for training and test on unrestored images at various distances from the focal plane of the camera. Defining the operational range as the distance up to which the error bars of the authentic and impostor scores do not overlap, we compare the approximate operational range of the iris recognition system both with and without the phase mask in Table I. We also compare the performance of the two different matching techniques (see Table II). Figs. 10 and 11 show the recognition results of conventional and wavefront-coded optical systems, respectively.

In the conventional case, the iriscodes algorithm seems to be performing better than the correlation-filter-based matching. This suggests that the iriscodes algorithm is more tolerant to normal blur, which changes with distance from the focal plane, compared to correlation filters since iriscodes uses only the phase information which is not adversely affected by normal blur. When using wavefront-coded imagery, we see that both iriscodes and correlation filters significantly increase the operational distance of the recognition system. Correlation filters perform slightly better than iriscodes as reflected in the larger operational range. This might be either due to robustness to segmentation errors or due to its better tolerance to the blurring caused by wavefront coding compared to the iriscodes algorithm (addressed in “Experiment III”). Tables III and IV compare the recognition performance when using wavefront-coding and conventional optics, respectively. Even though the increase in the depth of field of correlation filters over iriscodes may not appear to be large, the recognition performance of correlation filters is better than that of iriscodes over the range of the depth of field when wavefront-coded imagery is used. In fact, the recognition performance of correlation filters at the focal plane when using wavefront-coded imagery is as good as the recognition performance when using conventional images. The iriscodes algorithm, however, performs slightly worse because of its inability to fully tolerate the blurring caused by wavefront coding.

### B. Experiment I(b)

This is very similar to Experiment I(a), except that, while training, we use sample images at different distances (can be obtained from the in-focus image by simulation). For correlation-filter-based matching, a single fusion OTSDF filter uses all the training images, while in the case of iriscodes, a query is matched with all the training templates. Since the templates are trained using images from different distances, the algorithms are expected to perform better than in Experiment I(a) since the training set covers a greater range of image variation seen during testing. In our experiments, we use images at distances of  $-2$  to  $+2$  cm only from the focal plane in the template. We do not use images at larger distances in our template because poor segmentation at greater distances may affect the overall filter performance. For proper comparison, we use the same training sets for both iriscodes and correlation-filter-based matching.

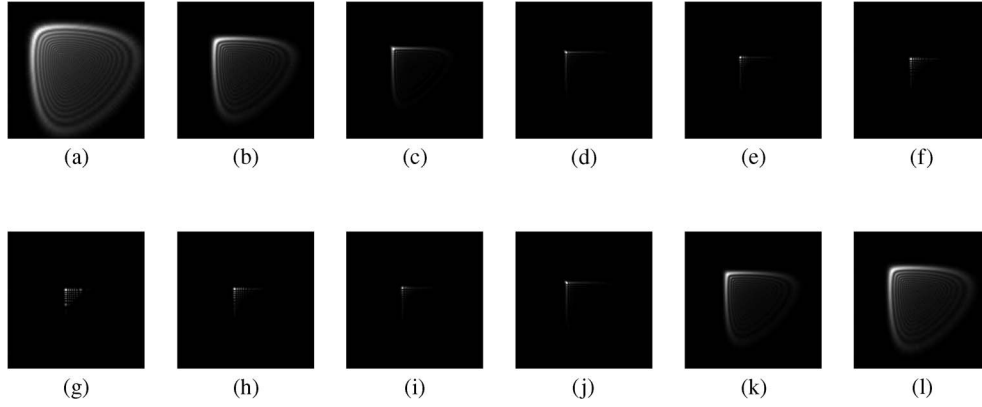


Fig. 9. PSF of a wavefront-coding system (cubic phase mask with  $\beta = 30$ ) over a range of 22 cm away from the focal plane. The shape of the PSF does not vary much from  $-5$  to  $+6$  cm. (a)  $-10$  cm. (b)  $-8$  cm. (c)  $-6$  cm. (d)  $-5$  cm. (e)  $-3$  cm. (f)  $-2$  cm. (g)  $0$  cm. (h)  $2$  cm. (i)  $3$  cm. (j)  $6$  cm. (k)  $10$  cm. (l)  $12$  cm.

TABLE I  
OPERATIONAL RANGE COMPARISON [EXPERIMENT I(a)]

Iriscode		
Data Type	Distance (in cm)	Operational Range (in cm)
Conventional	-2.9   2.9	$\sim 5.8$
Wavefront-Coded	-4.8   5.3	$\sim 10.1$
Correlation Filters		
Data Type	Distance (in cm)	Operational Range (in cm)
Conventional	-2.7   2.7	$\sim 5.4$
Wavefront-Coded	-6.1   6.5	$\sim 12.6$

TABLE II  
OPERATIONAL RANGE IMPROVEMENT [EXPERIMENT I(a)]

Operational Range	Conventional (in cm)	Wavefront (in cm)	Improvement (Ratio)
Iriscode	5.8	10.1	$\sim 1.75$
Correlation Filters	5.4	12.6	$\sim 2.34$

Figs. 12 and 13 show the results of the conventional and wavefront-coded optical systems, respectively, and Tables V and VI compare the performance of both iriscode and correlation filters when using the two different imaging systems.

We can see an increase in the operational range in the case of iriscode. While this is not so apparent in the case of correlation filters, we notice an increase in the separation between the mean authentic and impostor scores for distances whose samples were used for training the filter. This suggests that including samples from other distances might further help increase the range. We pursue this further in “Experiment II.” We also notice that both correlation filters and iriscode perform better at distances slightly away from the focal plane than when the iris is in focus. This is due to the fact that small variations affect the appearance of the in-focus images more than they affect the slightly blurred images. When the images are slightly blurred, all the extraneous high-frequency effects like noise or other unwanted variations are smoothed out even while preserving the underlying iris texture pattern. This helps improve tolerance to slight variations, leading to better performance. Such an effect was also observed in fingerprint recognition with correlation filters [24] where higher resolution did not always yield better recognition accuracy. However, as the blurring increases, the

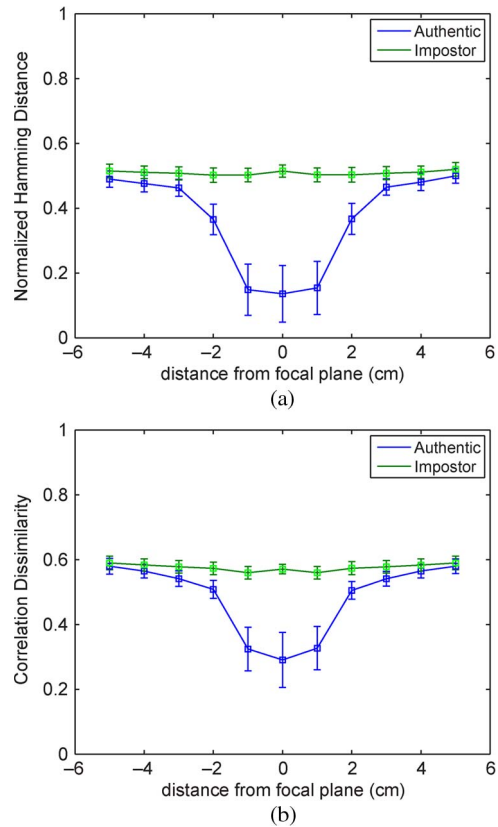


Fig. 10. Results of iriscode and correlation filters for the conventional optical system [Experiment I(a)]. (a) Iriscode on conventional images. (b) Correlation filters on conventional images.

recognition performance decreases as the texture detail starts disappearing.

C. Experiment II(a)

To quantify the matching performance alone and circumvent the effect of poor segmentation, in this experiment, we use the segmentation from the in-focus iris images to segment the unrestored wavefront-coded (cubic phase mask with  $\beta = 30$ ) images at different distances. The results in this experiment are expected to be better than those in “Experiment I,” since now, all the images are segmented using the same segmentation, and these results would be the best that one can hope for

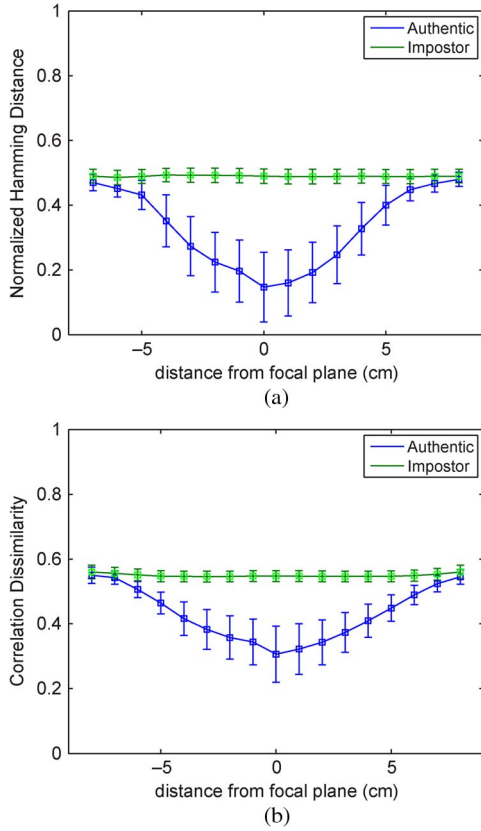


Fig. 11. Results of iriscode and correlation filters for the wavefront-coded optical system [Experiment I(a)]. (a) Iriscode on unrestored wavefront-coded images. (b) Correlation filters on unrestored wavefront-coded images.

TABLE III  
RECOGNITION RESULTS ON WAVEFRONT-CODED IMAGES [EXPERIMENT I(a)]

Distance (in cm)	Iriscode (FRR in %)		Correlation Filter (FRR in %)	
	FAR=1%	FAR=0.1%	FAR=1%	FAR=0.1%
-6 to 7	27.3	34.0	12.5	17.7
-5 to 5	12.3	17.0	2.80	4.70
-4 to 4	4.93	7.54	1.86	2.86
-3 to 3	2.34	3.43	1.48	2.21
-2 to 2	1.73	2.46	1.18	1.80
-1 to 1	2.16	2.30	1.00	1.60
0	1.50	1.90	0.45	1.00

TABLE IV  
RECOGNITION RESULTS ON CONVENTIONAL IMAGES [EXPERIMENT I(a)]

Range (in cm)	Iriscode (FRR in %)		Correlation Filter (FRR in %)	
	FAR=1%	FAR=0.1%	FAR=1%	FAR=0.1%
-4 to 4	39.2	47.6	42.1	53.4
-3 to 3	22.6	33.6	25.9	39.0
-2 to 2	2.80	6.02	7.94	12.4
-1 to 1	0.72	1.12	0.75	1.20
0	0.44	0.67	0.60	0.90

using unrestored wavefront-coded imagery. Fig. 14 shows the results of this experiment using both iriscode and correlation filters, and Table VII summarizes the depth of field for both the algorithms.

The depth of field for both iriscode and correlation filters is considerably larger compared to that in “Experiment I.” This

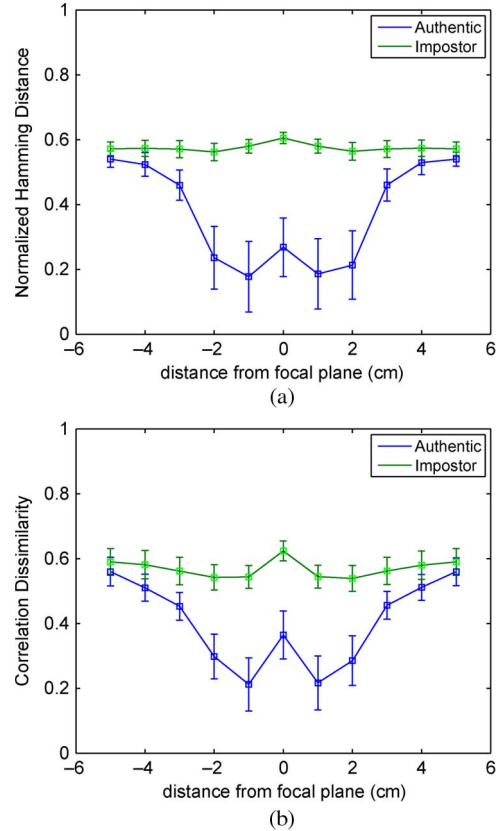


Fig. 12. Results of iriscode and correlation filters for the conventional optical system [Experiment I(b)]. (a) Iriscode on conventional images. (b) Correlation filters on conventional images.

goes to show that the smaller depth of field in “Experiment I” was more due to poor segmentation rather than due to the blurring caused by the wavefront-coding element. Table VIII shows the recognition performance over the depth of field. We can see that the recognition performance of both matching algorithms remains good from  $-5$  to  $5$  cm which incidentally is the range over which the PSF remains roughly invariant (see Fig. 9). At distances close to the focal plane, the correlation filter’s recognition performance is as good as that using conventional in-focus images, while iriscode performs slightly worse. However, at distances further away from the focal plane, the iriscode algorithm does better than correlation filters. This is due to the fact that, closer to the focal plane, the blurring is dominated by the cubic phase of the wavefront-coding element to which correlation filters are tolerant, while further away from the focal plane, the blurring is dominated by conventional blur of the lens to which iriscode is more tolerant. This property of the iriscode algorithm gives it slightly greater depth of field than correlation filters. Seen in this light, the results of “Experiment I” suggest that iriscode is more sensitive to segmentation errors, caused by the blurring, than correlation filters.

#### D. Experiment II(b)

This experiment is very similar to Experiment I(b) (cubic phase mask with  $\beta = 30$ ), except that we segment all the iris images using the segmentation at best focus. Fig. 15 and Table IX show the results of both iriscode and correlation filters

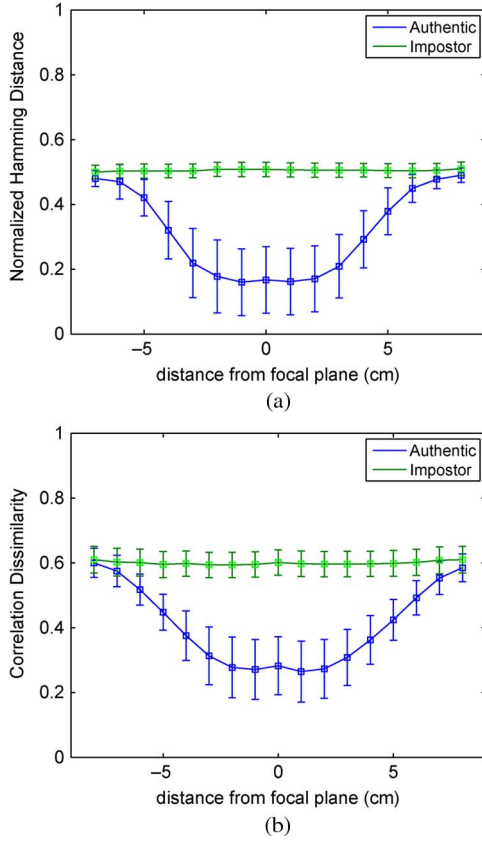


Fig. 13. Results of iriscodes and correlation filters for the wavefront-coded optical system [Experiment I(b)]. (a) Iriscodes on unrestored wavefront-coded images. (b) Correlation filters on unrestored wavefront-coded images.

TABLE V  
OPERATIONAL RANGE COMPARISON [EXPERIMENT I(b)]

Iriscodes			
Data Type	Distance (in cm)		Operational Range (in cm)
Conventional	-4.0	3.8	~7.8
Wavefront-Coded	-5.5	6.0	~11.5
Correlation Filters			
Data Type	Distance (in cm)		Operational Range (in cm)
Conventional	-3.6	3.5	~7.1
Wavefront-Coded	-5.9	6.3	~12.2

TABLE VI  
OPERATIONAL RANGE IMPROVEMENT [EXPERIMENT I(b)]

Operational Range	Conventional (in cm)	Wavefront (in cm)	Improvement (Ratio)
Iriscodes	7.8	11.5	~1.5
Correlation Filters	7.1	12.2	~1.7

on such images. In Experiment I(b), even though images at distances from  $-2$  to  $2$  cm were used for training, there was not any appreciable increase in the depth of field. This may be due to the fact that the PSF is constant over  $-2$  to  $2$  cm, leading to no performance improvement over Experiment 1(a). To test out this hypothesis, in this experiment, we use images at distances of  $-6$ ,  $0$ , and  $8$  cm for training. These were chosen since, at  $-6$  and  $8$  cm, the PSF is significantly different compared to the PSF at  $0$  cm, as shown in Fig. 9.

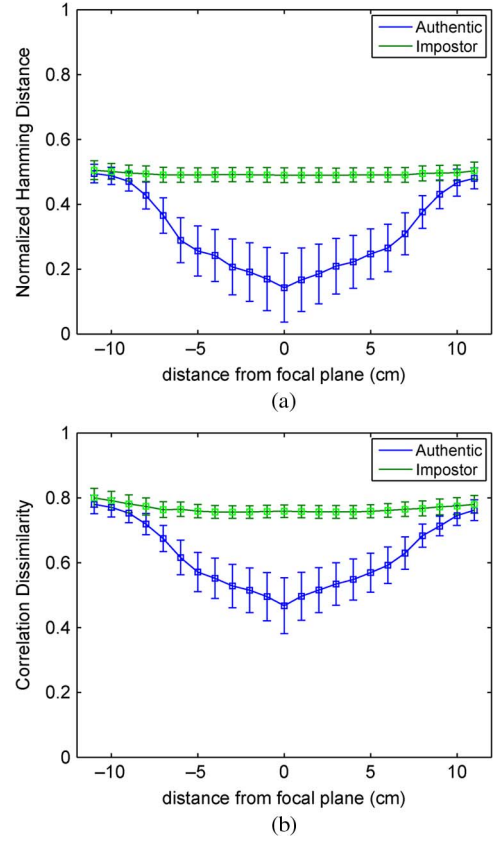


Fig. 14. Results of iriscodes and correlation filters for the wavefront-coded optical system [Experiment II(a)]. (a) Iriscodes on unrestored wavefront-coded images. (b) Correlation filters on unrestored wavefront-coded images.

TABLE VII  
OPERATIONAL RANGE COMPARISON [EXPERIMENT II(a)]

Data Type	Distance (in cm)		Operational Range (in cm)
Iriscodes	-7.9	9.1	~17.0
Correlation Filter	-7.9	9.0	~16.9

TABLE VIII  
RECOGNITION RESULTS FOR EXPERIMENT II(a)

Distance (in cm)	Iriscodes (FRR in %)		Correlation Filter (FRR in %)	
	FAR=1%	FAR=0.1%	FAR=1%	FAR=0.1%
-9 to 9	15.1	20.4	18.2	21.3
-7 to 7	2.13	4.20	3.23	5.87
-5 to 5	1.82	2.56	0.82	1.97
-3 to 3	1.60	2.23	0.55	1.25
-1 to 1	1.42	1.88	0.42	0.94
0	1.50	1.90	0.45	1.00

The results show an improvement of over 2 cm compared to using in-focus images only for training, which confirms our hypothesis and also shows that further gains in the depth of field can be had from using images at other distances also for training.

### E. Experiment III

In this experiment, to study the impact of the blurring caused by wavefront coding, we restore the wavefront-coded (cubic phase with  $\beta = 30$ ) images as is commonly done before

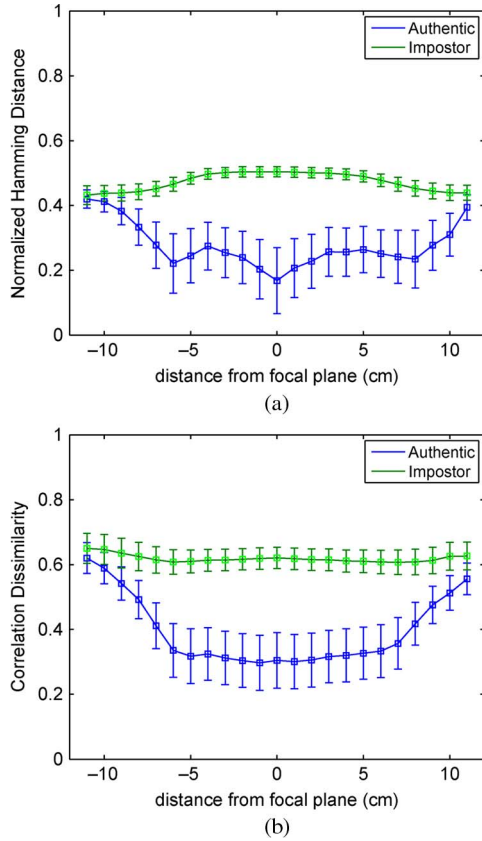


Fig. 15. Results of iriscodes and correlation filters for the wavefront-coded optical system [Experiment II(b)]. (a) Iriscodes on unrestored wavefront-coded images. (b) Correlation filters on unrestored wavefront-coded images.

TABLE IX  
OPERATIONAL RANGE COMPARISON [EXPERIMENT II(b)]

Data Type	Distance (in cm)	Operational Range (in cm)
Iriscodes	-8.8 10.7	~19.5
Correlation Filter	-8.8 10.5	~19.3

feeding those images to the iris recognition module. We use the Lucy–Richardson iterative algorithm [25], [26] to restore the wavefront-coded images. This technique requires an estimate of the PSF which cannot be obtained without knowing the exact distance of the iris from the focal plane of the lens. Hence, the restoration is done using the in-focus PSF. The fact that the PSF does not change its shape over a reasonable imaging volume (see Fig. 9) helps us achieve good image deconvolution, at least over that volume. Fig. 16 shows the results of iriscodes and correlation filters on restored wavefront-coded imagery while using segmentation from in-focus images, and Table X summarizes the depth of field for both the algorithms.

The depth of field for both the matching algorithms is much larger compared to that in Experiment I and slightly larger than that in Experiment II(a). However, the results are actually worse than those in Experiment II(b). This lends further credence to the fact that, as long as there are no segmentation errors, the recognition performance of both the algorithms on unrestored wavefront-coded imagery is almost as good as that on restored images at a lower computational cost. Table XI shows the

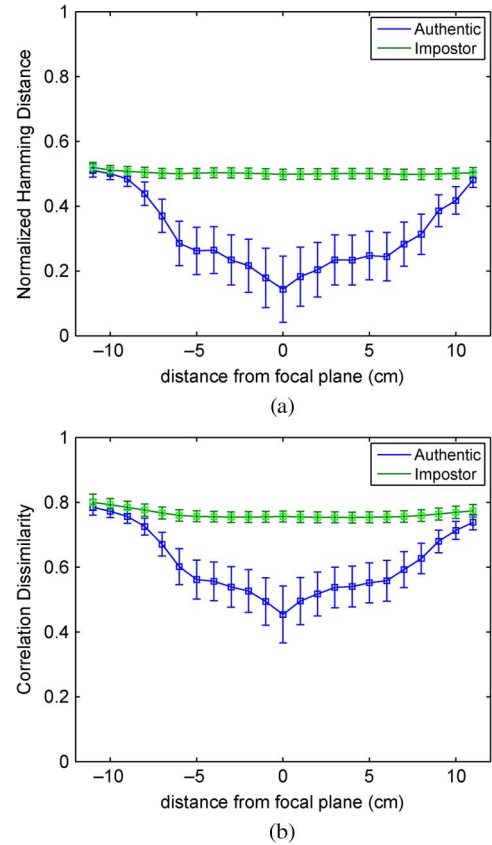


Fig. 16. Results of iriscodes and correlation filters for the wavefront-coded optical system (Experiment III). (a) Iriscodes on restored wavefront-coded images. (b) Correlation filters on restored wavefront-coded images.

TABLE X  
OPERATIONAL RANGE COMPARISON (EXPERIMENT III)

Data Type	Distance (in cm)	Operational Range (in cm)
Iriscodes	-8.5 10.5	~19.0
Correlation Filter	-8.4 10.3	~18.7

TABLE XI  
RECOGNITION RESULTS FOR EXPERIMENT III

Distance (in cm)	Iriscodes (FRR in %)		Correlation Filter (FRR in %)	
	FAR=1%	FAR=0.1%	FAR=1%	FAR=0.1%
-9 to 11	13.1	16.4	18.0	22.1
-7 to 7	1.86	3.12	2.41	3.72
-5 to 5	1.23	1.74	0.92	1.38
-3 to 3	1.08	1.42	0.70	1.23
-1 to 1	0.95	1.21	0.60	0.98
0	0.70	1.00	0.50	0.90

recognition performance over the different range of distances from the focal plane of the camera.

#### F. Experiment IV

In this experiment, we investigate the effect of the gain parameter of the cubic phase mask. We perform Experiment II(a) using images obtained by changing the gain parameter of the wavefront-coding element. Increasing the gain parameter causes the PSF of the camera system to be invariant over a larger distance, which would increase the effective depth of

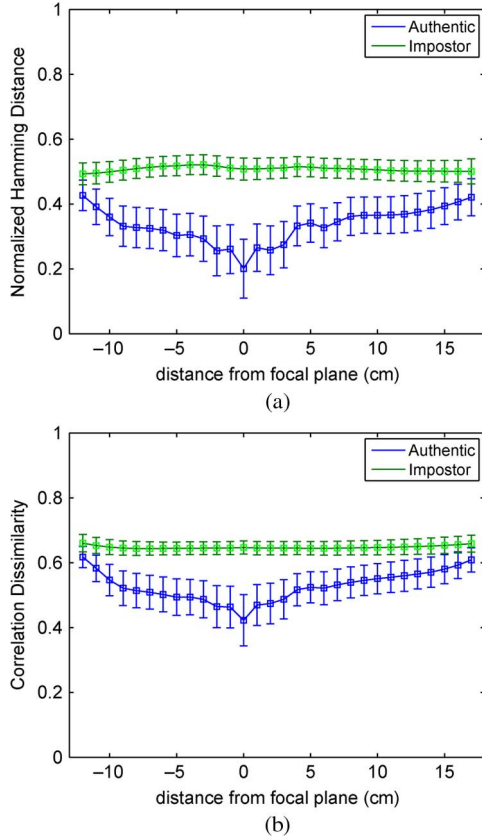


Fig. 17. Results of iriscodes and correlation filters for the wavefront-coded optical system (Experiment IV). (a) Iriscodes on restored wavefront-coded images. (b) Correlation filters on restored wavefront-coded images.

TABLE XII  
OPERATIONAL RANGE COMPARISON (EXPERIMENT IV)

Data Type	Distance (in cm)	Operational Range (in cm)
Iriscodes	-11.5   16.2	~27.7
Correlation Filter	-11.3   15.5	~26.8

field of the iris recognition system at the cost of performance degradation at best focus. To investigate this effect, we increase the gain parameter to  $\beta = 60$ . Fig. 17 shows the results of both iriscodes and correlation filters on the wavefront-coded imagery with larger gain parameter and using segmentation from images at best focus. Table XII summarizes the depth of field for both the algorithms.

As expected, the depth of field of the camera system increased on account of using a larger gain in the wavefront-coding element. However, the recognition performance at best focus is no longer as good as in Experiment II(a). Table XIII shows the recognition performance over different ranges of distances. While it would seem that, by increasing the gain of the wavefront-coding element, we can arbitrarily increase the depth of field, there is a tradeoff with the recognition performance at best focus.

### G. Experiment V

From the results of the previous experiments, we make the following observations.

TABLE XIII  
RECOGNITION RESULTS FOR EXPERIMENT IV

Distance (in cm)	Iriscodes (FRR in %)		Correlation Filter (FRR in %)	
	FAR=1%	FAR=0.1%	FAR=1%	FAR=0.1%
-12 to 17	13.8	22.8	15.5	23.1
-11 to 11	7.4	13.7	8.0	13.9
-9 to 9	4.94	9.84	5.10	9.71
-7 to 7	3.82	7.64	3.70	7.1
-5 to 5	3.33	6.32	2.83	5.53
-3 to 3	2.62	4.12	2.25	3.90
-1 to 1	2.40	4.17	1.88	3.30
0	1.94	2.62	1.36	1.82

- 1) The main challenge to increasing the operational range of iris recognition systems when using unrestored wavefront-coded imagery comes from iris segmentation which becomes increasingly difficult with increasing distance from the focal plane.
- 2) Improving the segmentation algorithm would enable us to use the full power of the matching techniques to get greater depth of field without modifying the existing matching techniques.
- 3) Correlation filters have good recognition performance as long as the PSF of the wavefront-coding system does not change drastically from training and testing.

Recently, Bagheri *et al.* [27] showed that a pure cubic phase mask is not the best solution for iris recognition because of the variation in image magnification as the iris moves along the optical axis. Furthermore, the separable form of the phase mask results in low modulation along the diagonals because of the asymmetric nature of the PSF. This also has an adverse impact on the segmentation algorithm which is an important factor affecting the achievable depth of field when using unrestored images. Using symmetric phase functions can help overcome both the aforementioned limitations. In light of the above observations, designing a custom phase mask which overcomes the aforementioned factors would help us increase the gain in depth of field while using unrestored wavefront-coded iris images. To this end, we also use a higher order phase function, a cubic-pentac function given by  $\phi(x, y) = a_1(x^3 + y^3) + a_2(x^2y + xy^2) + a_3(x^5 + y^5) + a_4(x^4y + xy^4) + a_5(x^3y^2 + x^2y^3)$ . This choice of the phase function is motivated by the following. (For a more detailed treatment on the advantages of using a higher order cubic-pentac for iris images, see [28].)

- 1) The extra degrees of freedom of the cubic-pentac over the cubic phase mask allows for less loss in information in the raw wavefront-coded images.
- 2) The nonseparable nature of the phase function enables us to design wavefront-coding elements such that the resulting PSF is circularly symmetric, which makes segmentation easier.
- 3) The extra degrees of freedom also allows the PSF to be invariant over a larger range of distances which helps correlation filters achieve a greater depth of field.

The coefficients of the phase mask  $\mathbf{a} = [a_1, a_2, a_3, a_4, a_5]$  are the design parameters for the phase mask which we solve for by setting up an optimization problem following the design

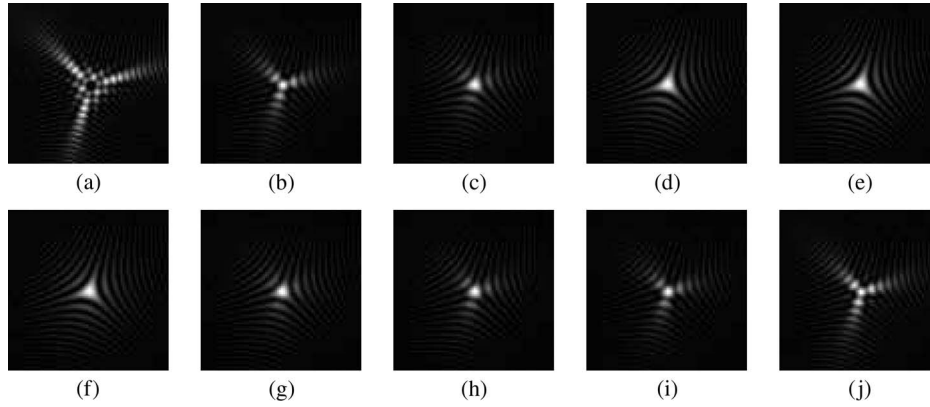


Fig. 18. PSF of a wavefront-coding system (cubic–pentic phase mask) over a range of 24 cm away from the focal plane. The shape of the PSF does not vary much from  $-5$  to  $+6$  cm. (a)  $-11$  cm. (b)  $-8$  cm. (c)  $-5$  cm. (d)  $-2$  cm. (e)  $0$  cm. (f)  $2$  cm. (g)  $6$  cm. (h)  $8$  cm. (i)  $10$  cm. (j)  $13$  cm.

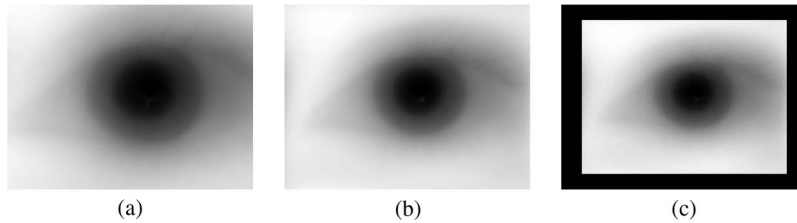


Fig. 19. Examples of iris images from the wavefront-coded system using the cubic–pentic phase mask. (a)  $-10$  cm. (b)  $0$  cm. (c)  $+10$  cm.

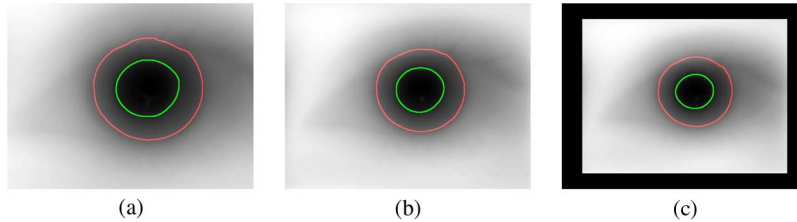


Fig. 20. Examples of iris segmentation for images from the wavefront-coded system using the cubic–pentic phase mask. (a)  $-10$  cm. (b)  $0$  cm. (c)  $+10$  cm.

procedure in [28], with minor modifications to reduce the computational complexity and also to more forcibly enforce the solution of the resulting PSF to be circularly symmetric

$$\mathbf{a} = \arg \min_{\mathbf{a}} w_D D(\mathbf{a}) + w_S S(\mathbf{a}) \quad (11)$$

where  $w_D$  and  $w_S$  are weights for the objective functions  $D(\mathbf{a})$  and  $S(\mathbf{a})$  defined as follows:

$$D(\mathbf{a}) = \left\| \frac{\partial^2}{\partial \tau^2} H(\mathbf{a}, u, v, 0) \right\|_E \approx \left( \sum_n \sum_m \left| \frac{\partial^2}{\partial \tau^2} H(\mathbf{a}, u_n, v_m, 0) \right|^2 \right)^{\frac{1}{2}} \quad (12)$$

$$S(\mathbf{a}) = \sum_{\rho_0 \in C} \sum_m |H(\mathbf{a}, \rho_0, \alpha_{\text{ref}}, 0) - H(\mathbf{a}, \rho_0, \alpha_m, 0)| \quad (13)$$

where  $H(\mathbf{a}, u, v, \tau)$  is the optical transfer function of the wavefront-coded system,  $(u, v)$  are the normalized spatial frequency variables,  $(\rho, \alpha)$  are the polar coordinates in the frequency plane  $(u, v)$ , and  $C$  is a random set of radii  $\rho$ .  $D(\mathbf{a})$  is the objective function which enforces the invariance of the optical transfer function to defocus, while  $S(\mathbf{a})$  is the objective function which forces the resulting PSF to be circularly symmetric. In our experiments, the weights  $w_D$  and  $w_S$  were

chosen such that the contributions from the two objective functions are of the same order. Since the solution space is densely populated with local minima, we use a Monte Carlo simulation by randomly generating tens of thousands of starting points and using the top 1% promising trials for optimization. All the coefficients  $a_i$ 's are restricted to  $-500 \leq a_i \leq 500$ . One solution obtained from our optimization with the least cost function is  $\mathbf{a} = [192.68, -488.75, 93.94, -423.80, -310.68]$ .

Fig. 18 shows the PSF of this custom-designed phase mask over a range of 24 cm away from the focal plane. Observe that the PSF remains mostly invariant to defocus over a large part of this range. Fig. 19 shows some images when using the designed cubic–pentic phase mask, and Fig. 20 shows the results of our segmentation algorithm on these images. We can see that, even at best focus, the image is fairly blurred; however, images at other distances look very similar to the image at best focus. It must also be noted that our segmentation algorithm performs reasonably even at distances far away from the focal plane due to the circular symmetry of the PSF, while it failed when segmenting images from the cubic phase mask at similar distance from the focal plane.

By using the images from the designed phase mask, we conduct Experiment I(a). Fig. 21 shows the results of both iriscodes and correlation filters when using the cubic–pentic

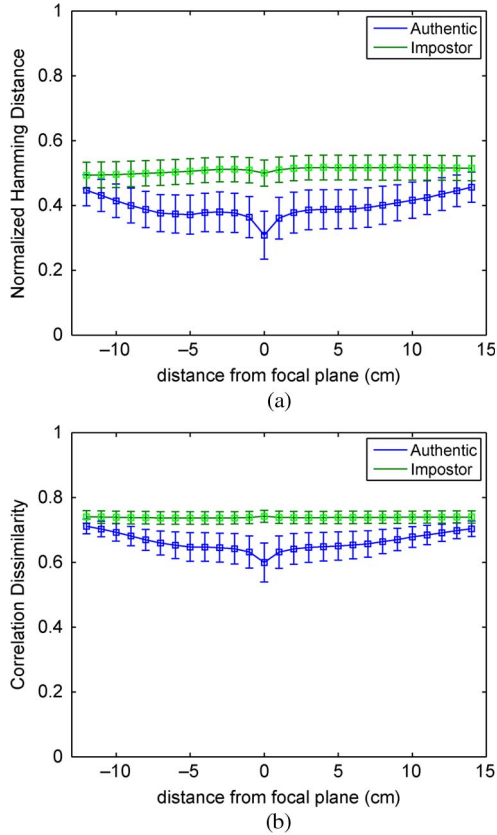


Fig. 21. Results of iriscode and correlation filters for the wavefront-coded optical system (Experiment V). (a) Iriscode on restored wavefront-coded images. (b) Correlation filters on restored wavefront-coded images.

TABLE XIV  
OPERATIONAL RANGE COMPARISON (EXPERIMENT V)

Data Type	Distance (in cm)		Operational Range (in cm)
Iriscode	-9.2	11.2	~20.4
Correlation Filter	-10.0	12.8	~22.8

TABLE XV  
RECOGNITION RESULTS FOR EXPERIMENT V

Distance (in cm)	Iriscode (FRR in %)		Correlation Filter (FRR in %)	
	FAR=1%	FAR=0.1%	FAR=1%	FAR=0.1%
-10 to 12	28.5	45.4	20.6	36.0
-9 to 9	24.2	40.3	16.5	30.4
-7 to 7	21.5	36.9	13.9	26.4
-5 to 5	20.3	35.3	12.5	24.1
-3 to 3	19.1	33.2	10.9	21.4
-1 to 1	14.0	25.4	7.4	15.3
0	8.2	14.5	3.8	8.7

phase mask. Table XIV summarizes the depth of field for both the algorithms, and Table XV shows the recognition performance over different ranges of distances.

As expected, the depth of field of the camera system increased greatly over a conventional camera system. The operational range in this case is larger than that in Experiment III, but the recognition performance at best focus is no longer as good as that in Experiment II(a). This can be explained by the fact that, while designing the phase mask, the constraints we used were only on the circular symmetry of the phase mask and

TABLE XVI  
SUMMARY OF RESULTS: GAIN IN DEPTH OF FIELD IS THE RATIO OF THE DEPTH OF FIELD ACHIEVED BY WAVEFRONT CODING TO THE DEPTH OF FIELD OF A CONVENTIONAL CAMERA FOR EACH ALGORITHM (GIVEN BELOW THE NAME OF THE ALGORITHM, CORRELATION FILTERS ABBREVIATED AS CF)

Operational Range	Wavefront (in cm)		Gain (ratio)	
	Iriscode (5.8cm)	CF (5.4cm)	Iriscode	CF
Unrestored	~ 10.1	~ 12.6	~ 1.8	~ 2.3
Unrestored-correct segment	~ 17.0	~ 16.9	~ 2.9	~ 3.1
Unrestored-correct segment (train with multiple distances)	~ 19.5	~ 19.3	~ 3.6	~ 3.5
Restored-correct segment	~ 19.0	~ 18.7	~ 3.3	~ 3.5
Unrestored-correct segment (with $\beta = 60$ )	~ 27.7	~ 26.8	~ 4.8	~ 5.0
Unrestored (optimized cubic-pentic)	~ 20.4	~ 22.8	~ 3.5	~ 4.2

invariance to defocus and that there was no explicit constraint on the acceptable amount of blurring at best focus. However, adding such a constraint would compromise the circular symmetry of the phase mask and also the invariance to defocus. Therefore, this delicate tradeoff needs to be made on a case-by-case basis depending on the performance of the segmentation and matching algorithm.

Table XVI summarizes the results of all our experiments for extending the depth of field of iris recognition systems.

## VII. CONCLUSION

Iris recognition technology can achieve very high matching accuracy but still requires substantial user cooperation. To ease this requirement on the user, we require that the operational range of the iris acquisition system be larger than what it is today. Wavefront coding offers a solution to achieve this, but there have not been any large-scale tests to quantify and confirm the increase in the depth of field that can be achieved. In this paper, we have addressed this problem by using a very large set of simulated wavefront-coded images for evaluation. We have also carefully investigated the feasibility of using unrestored wavefront-coded images for recognition since this helps reduce the computational cost associated with image restoration and also by the fact that the recognition performance, both in terms of recognition accuracy and depth of field, is only slightly worse than the recognition performance on restored images. Overall, our experimental results show that wavefront coding can help us increase the depth of field of an iris recognition system by a factor of four.

## ACKNOWLEDGMENT

The authors would like to thank the anonymous reviewers for their constructive reviews of an earlier version of this paper. This work was supported in part by the Army Research Office (ARO) support to CyLab at Carnegie Mellon University.

## REFERENCES

- [1] E. R. Dowski and W. T. Cathey, "Extended depth of field through wavefront coding," *Appl. Opt.*, vol. 34, no. 11, pp. 1859–1866, Apr. 1995.
- [2] W. T. Cathey and E. R. Dowski, "New paradigm for imaging systems," *Appl. Opt.*, vol. 41, no. 29, pp. 6080–6092, Oct. 2002.

- [3] A. Mahalanobis, B. V. K. Vijaya Kumar, and D. Casasent, "Minimum average correlation energy filters," *Appl. Opt.*, vol. 26, no. 17, pp. 3633–3640, Sep. 1987.
- [4] M. Savvides, B. V. K. Vijayakumar, and P. K. Khosla, "Cancelable biometric filters for face recognition," in *Proc. Int. Conf. Pattern Recog.*, 2004, pp. 922–925.
- [5] J. Daugman, "How iris recognition works," in *Proc. Int. Conf. Image Process.*, 2002, vol. 1, pp. 33–36.
- [6] J. Daugman, "New methods in Iris recognition," *IEEE Trans. Syst., Man, Cybern. B, Cybern.*, vol. 37, no. 5, pp. 1167–1175, Oct. 2007.
- [7] J. Daugman, "High confidence visual recognition of persons by a test of statistical independence," *IEEE Trans. Pattern Anal. Mach. Intell.*, vol. 15, no. 11, pp. 1148–1161, Nov. 1993.
- [8] R. Plemmons, M. Horvath, E. Leonhardt, P. Pauca, S. Prasad, S. Narayanswamy, and P. E. X. Silveira, "Computational imaging systems for Iris recognition," *Proc. SPIE*, vol. 5559, pp. 346–357, 2004.
- [9] R. Narayanswamy, G. E. Johnson, P. E. X. Silveira, and H. Wach, "Extending the imaging volume for biometric iris recognition," *Appl. Opt.*, vol. 44, no. 5, pp. 701–712, Feb. 2005.
- [10] K. N. Smith, V. P. Pauca, A. Ross, T. Torgersen, and M. C. King, "Extended evaluation of simulated wavefront coding technology in Iris recognition," in *Proc. IEEE BTAS*, 2007, pp. 1–7.
- [11] J. Thronton, "Matching deformed and occluded iris patterns: A probabilistic model based on discriminative cues," Ph.D. dissertation, Carnegie Mellon Univ., Pittsburgh, PA, 2007.
- [12] Iris Challenge Evaluation (ICE), [Online]. Available: <http://iris.nist.gov/ICE>
- [13] T. F. Chan and L. A. Vese, "Active contours without edges," *IEEE Trans. Image Process.*, vol. 10, no. 2, pp. 266–277, Feb. 2001.
- [14] J. Thronton, M. Savvides, and B. V. K. Vijaya Kumar, "An evaluation of Iris pattern representation," in *Proc. IEEE BTAS*, 2007, pp. 1–6.
- [15] C. F. Hester and D. Casasent, "Multivariate technique for multiclass pattern recognition," *Appl. Opt.*, vol. 19, no. 11, pp. 1758–1761, Jun. 1980.
- [16] B. V. K. Vijaya Kumar and A. Mahalanobis, "Recent advances in composite correlation filter designs," *Asian J. Phys.*, vol. 8, no. 3, pp. 407–420, 1999.
- [17] B. V. K. Vijaya Kumar, "Tutorial survey of composite filter designs for optical correlators," *Appl. Opt.*, vol. 31, no. 23, pp. 4773–4801, Aug. 1992.
- [18] B. V. K. Vijaya Kumar, D. W. Carlson, and A. Mahalanobis, "Optimal trade-off synthetic discriminant function filters for arbitrary devices," *Opt. Lett.*, vol. 19, no. 19, pp. 1556–1558, Oct. 1994.
- [19] B. V. K. Vijaya Kumar, M. Savvides, K. Venkataramani, and C. Xie, "Spatial frequency domain image processing for biometric recognition," in *Proc. Int. Conf. Image Process.*, 2002, pp. 53–56.
- [20] M. Savvides and B. V. K. Vijaya Kumar, "Efficient design of advanced correlation filters for robust distortion-tolerant face recognition," in *Proc. IEEE Conf. Adv. Video Signal Based Surveillance*, 2003, pp. 45–52.
- [21] J. Thronton, M. Savvides, and B. V. K. Vijaya Kumar, "Robust Iris recognition using advanced correlation techniques," in *Proc. Int. Conf. Image Anal. Recog.*, 2005, vol. 3656, pp. 1098–1105.
- [22] A. Mahalanobis and B. V. K. Vijaya Kumar, "Polynomial filters for higher-order correlation and multi-input information fusion," in *Proc. 11th Euro-Amer. Workshop, SPIE*, 1997, pp. 221–231.
- [23] A. K. Jain, *Fundamentals of Digital Image Processing*. Englewood Cliffs, NJ: Prentice-Hall, 1989, ser. Information and System Sciences.
- [24] K. Venkataramani and B. V. K. Vijaya Kumar, "Performance of composite correlation filters for fingerprint verification," *Opt. Eng.*, vol. 43, no. 8, pp. 1820–1827, Aug. 2004.
- [25] W. H. Richardson, "Bayesian-based iterative method of image restoration," *J. Opt. Soc. Amer.*, vol. 62, no. 1, pp. 55–59, Jan. 1972.
- [26] L. B. Lucy, "An iterative technique for the rectification of observed distributions," *Astron. J.*, vol. 79, no. 6, pp. 745–754, Jun. 1974.
- [27] S. Bagheri, P. E. X. Silveira, R. Narayanswamy, and D. P. de Farias, "Analytical optical solution of the extension of the depth of field using cubic-phase wavefront coding. Part II. Design and optimization of the cubic phase," *J. Opt. Soc. Amer. A, Opt. Image Sci.*, vol. 25, no. 5, pp. 064–1074, May 2008.
- [28] S. Barwick, "Increasing the information acquisition volume in iris recognition systems," *Appl. Opt.*, vol. 47, no. 26, pp. 4684–4691, Sep. 2008.



**Vishnu Naresh Boddeti** (S'08) received the B.Tech. degree in electrical engineering from the Indian Institute of Technology, Madras, India, in 2007 and the M.Sc. degree from Carnegie Mellon University, Pittsburgh, PA, where he is currently working toward the Ph.D. degree.

He is currently in the Electrical and Computer Engineering program at Carnegie Mellon University. His research interests are in computer vision, pattern recognition, and machine learning.



**B. V. K. Vijaya Kumar** (S'78–M'80–SM'90–F'10) received the B.Tech and M.Tech degrees in electrical engineering from the Indian Institute of Technology, Kanpur in 1975 and 1977, respectively. He received the Ph.D. degree in electrical engineering from Carnegie Mellon University in 1980.

He is currently a Professor with the Department of Electrical and Computer Engineering (ECE), Carnegie Mellon University (CMU), Pittsburgh, PA. His publications include the book entitled *Correlation Pattern Recognition* (coauthored with

Dr. A. Mahalanobis and Dr. R. Juday, Cambridge University Press, 2005), eight book chapters, and about 400 technical papers. His research interests include automatic target recognition algorithms, biometric recognition methods and coding, and signal processing for data storage systems.

Prof. Kumar is a Fellow of SPIE—the International Society of Optical Engineering, a Fellow of the Optical Society of America, and a Fellow of the International Association of Pattern Recognition. He has served as the Pattern Recognition Topical Editor for the Information Processing division of *Applied Optics* and is currently serving as an Associate Editor for the IEEE TRANSACTIONS ON INFORMATION FORENSICS AND SECURITY. He has served on many conference program committees and was a Cogeneral Chair of the 2004 Optical Data Storage Conference and a Cogeneral Chair of the 2005 IEEE AutoID Workshop. He was the recipient of the Eta Kappa Nu Award for Excellence in Teaching in the Department of ECE, CMU, in 2003 and the Carnegie Institute of Technology's Dowd Fellowship for educational contributions.